Solid-State Electronics 200 (2023) 108522

Contents lists available at ScienceDirect

Solid State Electronics

journal homepage: www.elsevier.com/locate/sse

Modeling thermal effects in STT-MRAM ☆

Tomáš Hadámek [a,*], Siegfried Selberherr [b], Wolfgang Goes [c], Viktor Sverdlov [a]

[a] Christian Doppler Laboratory for Nonvolatile Magnetoresistive Memory and Logic at the Institute for Microelectronics, TU Wien, Gußhausstraße 27-29, A-1040 Wien, Austria

[b] Institute for Microelectronics, TU Wien, Gußhausstraße 27-29, A-1040 Wien, Austria

[c] Silvaco Europe Ltd., Cambridge, United Kingdom

ARTICLE INFO

Keywords:
Stochastic Landau–Lifschitz–Gilbert equation
Spintronics
STT-MRAM
Temperature scaling
Statistical switching

ABSTRACT

We employ the stochastic Landau–Lifschitz–Gilbert (sLLG) equation to explore thermal effects on switching in the spin-transfer torque magnetoresistive random access memory (STT-MRAM). The distribution of the switching times depends on the meshes used for the discretization within the finite element method (FEM) implementation and we introduce an effective temperature scaling in the thermal field calculation to mitigate the switching time distribution dependencies on the element size. Furthermore, we investigate the switching statistics of the STT-MRAM at different temperatures and show that the switching time distribution has a lower mean value, but possesses a longer tail of long switching times for the higher operating temperatures. As a result, the STT-MRAM switching with a fixed voltage pulse duration becomes more error-prone at elevated temperatures.

1. Introduction

Spin-transfer torque magnetoresistive random access memory (STT-MRAM) is one of the promising candidates for a new memory technology due to its non-volatility, wide temperature operation range, CMOS compatibility [1,2], high-density integration capability, and the possibility for in-memory logic and computing [3]. During the STT-MRAM switching [4], high currents can pass through the structure, which results in an increased temperature and mediates the switching [5]. Moreover, the non-uniform magnetization of the free layer (FL) causes the current density to be inhomogeneous [6]. Even though STT-MRAM is now commercially available, fully-fledged three-dimensional (3D) computer-aided design tools are missing. We present a 3D finite element tool which enables the simulation of complex STT-MRAM structures, such as multi-FL structures, at finite temperature.

Due to the typical dimensions of the systems, atomistic simulations are not feasible and micromagnetic approach must be employed. The basis of the method is the Landau–Lifschitz–Gilbert (LLG) equation.

$$\frac{\partial \mathbf{m}}{\partial t} = -\gamma \mu_0 \mathbf{m} \times \mathbf{H}_{\text{eff}} + \alpha \mathbf{m} \times \frac{\partial \mathbf{m}}{\partial t} + \frac{1}{M_S} \mathbf{T}_S \tag{1}$$

$\mathbf{m}$ stands for the normalized magnetization, M_S is the saturation magnetization, γ, μ_0 and α are the gyromagnetic ratio, vacuum permeability and Gilbert damping respectively, $\mathbf{T}_S$ is a spin torque acting on the magnetization, and $\mathbf{H}_{\text{eff}}$ is the effective field. To account for the finite temperature, a random thermal field can be added to the effective field — resulting in the so-called sLLG equation. This is a so-called Langevin approach [7] which accounts for statistical variations at switching.

We employ the finite element method (FEM) to solve the sLLG equation coupled to spin and charge transport to investigate the switching statistics of the STT-MRAM cell at different temperatures. However, the results depend on the mesh size [8]. Although the dependencies of the saturation magnetization, the magnetic anisotropy, and the exchange interaction on temperature can be obtained within the sLLG approach, the sLLG equation does not give correct temperature dependencies [9,10], and an appropriate mesh- and/or temperature-dependent scaling of the parameters must be applied. In [8] the parameters of the sLLG were re-scaled to achieve mesh-independent simulations of ferromagnetic resonance. Here we use a scaling approach to the random thermal field in order to mitigate the element size influence on the switching dynamics.

2. Methods

In order to simulate the switching of STT-MRAM, magnetization, charge and spin dynamics have to be modeled simultaneously. When a voltage is applied across the structure, current starts flowing through the STT-MRAM cell and gets polarized in the first magnetic layer. The

☆ The review of this paper was arranged by Francisco Gamiz.

* Corresponding author.
E-mail address: tomashadamek@iue.tuwien.ac.at (T. Hadámek).

https://doi.org/10.1016/j.sse.2022.108522

Available online 16 November 2022

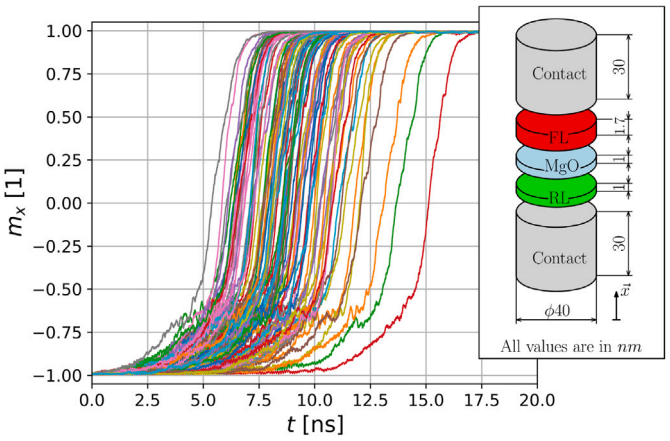

Fig. 1. Switching simulations for a shallow mesh. Thermalization of 2 ns is considerable before a voltage of −1 V across the structure is applied. The structure temperature is set to 300 K. Due to the finite temperature and random thermal fluctuations, switching time distribution is observed. Inset shows the simulated MRAM cell.

spin polarized current then exerts a moment on the second magnetic layer, which affects its magnetization. We solve the Poisson equation for the electric potential [11] and utilize the spin drift diffusion to determine the spin accumulation S. The spin accumulation determines the spin torques as

$$\mathbf{T}_{\mathrm{S}} = -\frac{D_e}{\lambda_J^2}\mathbf{m}\times\mathbf{S} - \frac{D_e}{\lambda_\varphi^2}\mathbf{m}\times(\mathbf{m}\times\mathbf{S}), \tag{2}$$

where D_e is the electron diffusion coefficient, λ_φ and λ_J are the spin dephasing and exchange lengths.

The magnetization is modeled with the LLG equation (1), with the effective field

$$\mathbf{H}_{\mathrm{eff}} = \mathbf{H}_{\mathrm{exg}} + \mathbf{H}_{\mathrm{aniso}} + \mathbf{H}_{\mathrm{demag}} + \mathbf{H}_{\mathrm{ext}} + \mathbf{H}_{\mathrm{th}}. \tag{3}$$

The terms in (3) stand for the exchange, anisotropy, demagnetization, external, and thermal field contributions, respectively. The demagnetization field is computed by a hybrid finite element-boundary element method approach [12]. For a finite element with indices i, j in the discretized FL, the random thermal field $\mathbf{H}_{\mathrm{th}}$ is assumed to have white noise characteristics and is uncorrelated in space and time t.

$$\left\langle \mathbf{H}_{\mathrm{th},i}(t), \mathbf{H}_{\mathrm{th},j}(t')\right\rangle = 2\frac{\alpha k_{\mathrm{B}} T_i}{\gamma\mu_0 M_{\mathrm{S}} V_i}\delta_{ij}\delta(t-t') \tag{4}$$

k_{B} is the Boltzmann constant, T_i and V_i are the element temperature and volume, and δ_{ij} and $\delta(t-t')$ are the Kronecker delta and Dirac delta function, respectively. The probability distribution function of the randomly generated numbers is Gaussian. To mitigate the influence of the element size on the switching at finite temperature, we follow [13], where the local effective temperature was introduced to tackle the nonphysical behavior. In the simulation, a scaled temperature T_i^{sim} in (4) is used instead of T_i. We generalized the approach [13] to account for the tetrahedral element shape by summing over all surface areas $S_{i,k}^{\mathrm{sim}}$ of the element.

$$T_i^{\mathrm{sim}} = T_i \frac{6 S_i V_i^{\mathrm{sim}}}{\sum_{k=1}^{4} S_{i,k}^{\mathrm{sim}} V_i} \tag{5}$$

The element volume and the side surface area are denoted by V_i^{sim} and S_i^{sim}. V_i and S_i are the volume and the side surface area of the unit lattice cell of the real magnetic material considered. T_i is set to the FL temperature.

We use the simulation parameters listed in Table 1 and the Backward Euler method for time integration.

Table 1
Simulation parameters.

Tunnel magnetoresistance ratio (TMR)	200%
Gilbert damping, α	0.02
Gyromagnetic ratio, γ	$1.76\cdot10^{-11}$ rad s^{-1}T^{-1}
Saturation magnetization, M_{S}	$1.2\cdot10^{-6}$ Am^{-1}
Exchange constant, A	$1\cdot10^{-11}$ Jm^{-1}
Anisotropy constant, K	$0.9\cdot10^{6}$ Jm^{-3}
Current spin polarization, β_σ	0.7
Diffusion spin polarization, β_{D}	1.0
Electron diffusion coefficient, D_e	$1\cdot10-4\,\mathrm{m}^2/\mathrm{s}$
Spin-flip length, λ_{sf}	10 nm
Spin dephasing length, λ_φ	0.4 nm
Exchange length, λ_J	0.5 nm

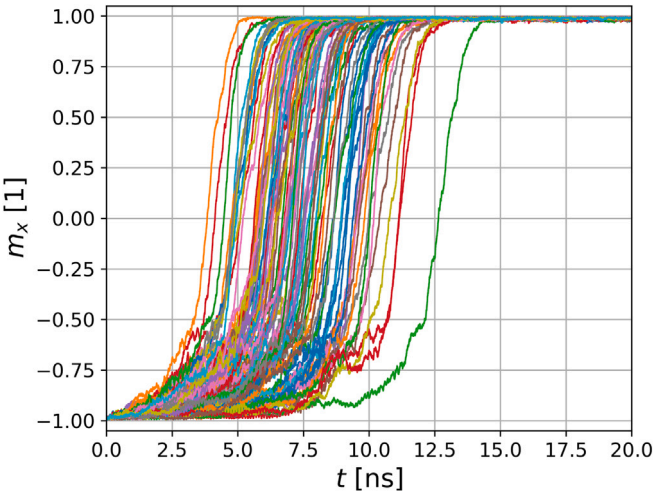

Fig. 2. Switching simulations with temperature scaling involved. Thermalization of 2 ns is considered before a voltage of −1 V across the structure is applied. The structure temperature is set to 300 K.

3. Results

We simulate a 5-layer cylindrical STT-MRAM cell with a diameter of 40 nm. The FeCoB reference layer (RL), the FeCoB FL and the MgO layer have thicknesses 1, 1.7 and 1 nm, respectively. The contacts are 30 nm long. The inset in Fig. 1 shows the described geometry in an exploded view. To investigate the mesh size dependence we employ two different mesh types. A "regular" mesh uses almost equilateral tetrahedral elements, whereas a "shallow" mesh uses elements with elongated lateral dimensions. The number of element layers within the FL is the same for both meshes. The regular mesh has about twice as many elements in the FL, hence the volume ratio is approximately equal to two. We run 100 switching simulations from an anti-parallel to parallel magnetization arrangement for both meshes, with and without temperature scaling using (5). The applied voltage is −1 V and the FL temperature is set to 300 K. For the simulation with the temperature scaling applied according to (5), V_i is set to be the volume of a unit cell with a lattice constant a = 2.5 Å, similar to the lattice constant of FeCoB. V_i^{sim} corresponds to the volume of the finite element with index i.

Figs. 1 and 2 show 100 realizations of the switching simulations at 300 K for the shallow mesh, with and without the temperature scaling (5) involved. An average magnetization m_x of the FL in the direction of the cylinder axis is shown. A result without the thermal field is omitted as the cell did not switch within the 20 ns simulation time window. Fig. 3 shows a histogram of switching times obtained for the different simulations. The threshold for completing the switching is set to 0.8 m_{x}. To make the results better visible, in Fig. 4, the histogram data is fitted

Table 2
First four statistical moment for the obtained Pearson IV distribution fits. The first 4 lines correspond to data from Fig. 4. The last 2 lines correspond to the data from Fig. 7.

	μ [ns]	σ [ns]	Skewness	Kurtosis
Regular	8.07	1.92	0.51	3.49
Regular, S.	7.33	2.07	1.19	5.29
Shallow	8.60	1.85	0.77	4.32
Shallow, S.	7.23	1.92	0.74	4.00
350 K	8.10	1.52	2.03	9.99
300 K	8.16	1.67	1.36	6.58

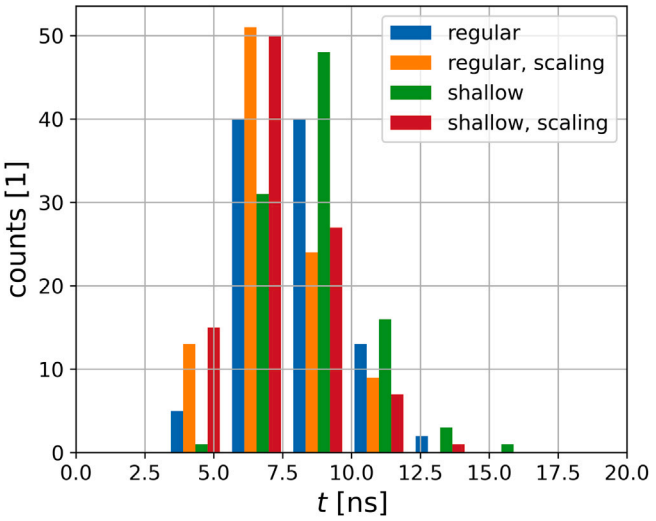

Fig. 3. Switching times for a structure with different element sizes with both, no temperature scaling and temperature scaling included. The switching threshold was set to +0.8 of the average free layer magnetization m_x.

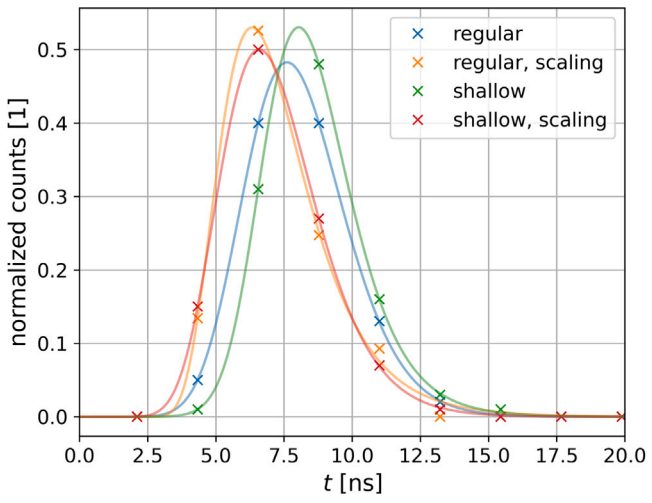

Fig. 4. Pearson Type IV distribution fitted to the switching times. The scaled simulations significantly mitigate the differences between the two different meshes.

with a Pearson Type IV distribution [14]. The simulations with scaled temperature strongly mitigate the result difference between the two meshes. Table 2 lists the first four statistical moments of the fitted distributions. The scaled simulations show a significantly improved match of the mean switching time μ. The standard deviation σ shows a slight increase for both meshes, when the temperature is scaled. The skewness and kurtosis do not show any apparent trend, but remain within the values reported in [14].

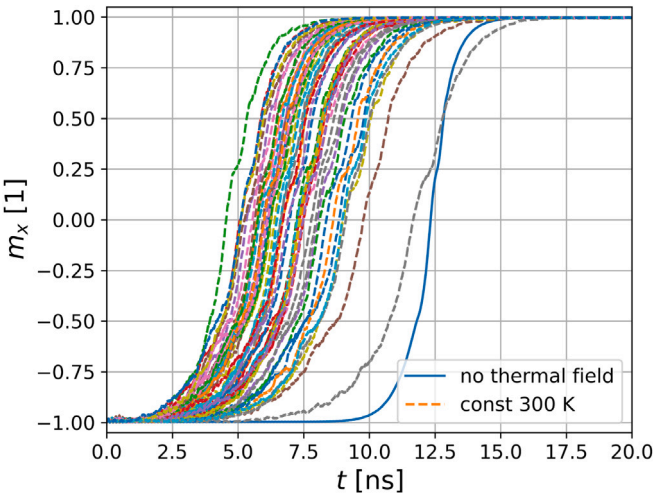

Fig. 5. Switching behavior at 300 K. The dashed lines represent 100 realizations of the switching at 300 K, whereas the solid line represents switching without any random thermal field added (switching at 0 K).

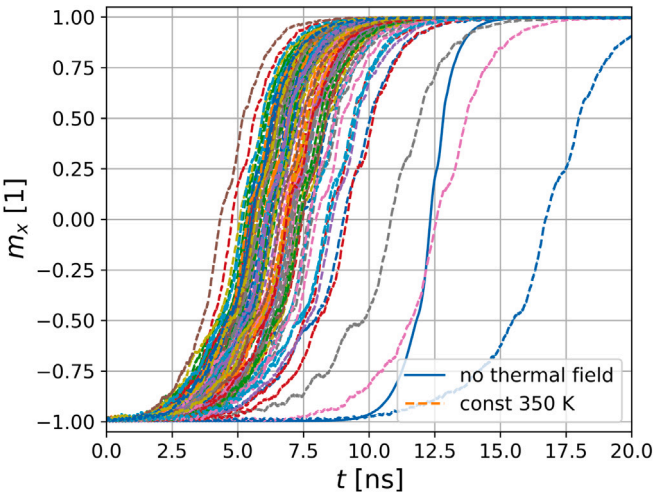

Fig. 6. Switching behavior at 350 K. The dashed lines represent 100 realizations of the switching at 350 K, whereas the solid line represents switching without any random thermal field added (switching at 0 K).

We further investigate the finite temperature effects on the switching of the STT-MRAM. Figs. 5 and 6 show the switching behavior with −2 V applied across the structure at constant temperatures of 300 and 350 K, respectively. The voltage is applied after 2 ns to allow magnetic layer thermalization. 100 numerical switching experiments are shown in dashed lines, whereas a solid line is used to identify a simulation without the thermal field included (switching at 0 K). The switching at 350 K is clearly faster for the majority of the experiments due to stronger thermal fluctuations resulting in a shorter initial switching phase. However, several switching paths possess slower switching times than the one at 0 K. The distribution of the switching times can be seen in Fig. 7. The lower switching times of the majority of experiments is clearly visible and further confirmed in Table 2 by slightly lower μ and lower σ of the corresponding Pearson IV data fits. On the other hand, the stronger fluctuations stabilize some of the switching experiments, resulting in a longer tail of slow switching times, represented by larger skewness and kurtosis of the distribution. The prolonged tail at 350 K

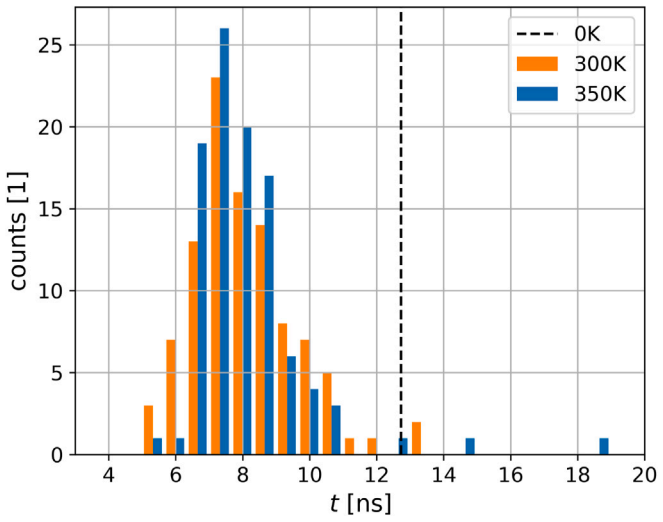

Fig. 7. Histogram of switching times for 300 and 350 K. The higher temperature reduces the mean switching time, however, a longer tail of long switching times can be observed. The switching time with no thermal field (0 K) is indicated by the black dashed line.

would lead to less reliable switching, when a voltage pulse with a finite length is used.

4. Conclusion

In this work, the sLLG equation is utilized to investigate the switching time distribution in the STT-MRAM at finite temperatures. It is demonstrated that the switching statistics obtained with solving the sLLG equation with the random thermal field depend on the meshes and the element mesh sizes. By introducing a mesh dependent local effective simulation temperature the switching time distributions are cease to depend on the mesh types. We further show that for elevated temperatures, a broader distribution of switching times at a fixed voltage is observed. The stronger thermal fluctuations cause the mean of the switching times to be lower, however, a longer tail of slow switching times is present, which leads to less reliable switching of the STT-MRAM, when a finite voltage pulse is applied.

Declaration of competing interest

The authors declare that they have no known competing financial interests or personal relationships that could have appeared to influence the work reported in this paper.

Data availability

Data will be made available on request.

Acknowledgments

The authors would like to acknowledge the financial support from the Austrian Federal Ministry for Digital and Economic Affairs, the National Foundation for Research, Technology and Development, the Christian Doppler Research Association and the TU Wien Bibliothek through its Open Access Funding Program.

References

[1] Ohno H. A hybrid CMOS/Magnetic tunnel junction approach for nonvolatile integrated circuits. In: 2009 Symposium on VLSI technology. IEEE; 2009, p. 122–3.
[2] Joshi VK, Barla P, Bhat S, Kaushik BK. From MTJ device to hybrid CMOS/MTJ circuits: A review. IEEE Access 2020;8:194105–46.
[3] Suzuki D, Natsui M, Mochizuki A, Miura S, Honjo H, Sato H, et al. Fabrication of a 3000-6-input-LUTs embedded and block-level power-gated nonvolatile FPGA chip using p-MTJ-based logic-in-memory structure. In: 2015 Symposium on VLSI circuits. 2015, p. C172–3. http://dx.doi.org/10.1109/VLSIC.2015.7231371.
[4] Cubukcu M, Boulle O, Drouard M, Garello K, Onur Avci C, Mihai Miron I, et al. Spin-orbit torque magnetization switching of a three-terminal perpendicular magnetic tunnel junction. Appl Phys Lett 2014;104(4):042406.
[5] Prejbeanu IL, Kerekes M, Sousa RC, Sibuet H, Redon O, Dieny B, et al. Thermally assisted MRAM. Vol. 19. No. 16. IOP Publishing; 2007, http://dx.doi.org/10.1088/0953-8984/19/16/165218, 165218.
[6] Fiorentini S, Ender J, Selberherr S, de Orio R, Goes W, Sverdlov V. Coupled spin and charge drift-diffusion approach applied to magnetic tunnel junctions. Solid-State Electron 2021;186:108103. http://dx.doi.org/10.1016/j.sse.2021.108103.
[7] García-Palacios JL, Lázaro FJ. Langevin-dynamics study of the dynamical properties of small magnetic particles. Phys Rev B 1998;58(22):14937.
[8] Oezelt H, Qu L, Kovacs A, Fischbacher J, Gusenbauer M, Beigelbeck R, et al. Full-spin-wave-scaled stochastic micromagnetism for mesh-independent simulations of ferromagnetic resonance and reversal. Npj Comput Mater 2022;8(1):1–9.
[9] Tsiantos V, et al. The effect of the cell size in Langevin micromagnetic simulations. J Magn Magn Mater 2002;242–245:999–1001. http://dx.doi.org/10.1016/S0304-8853(01)01365-8, Proceedings of the Joint European Magnetic Symposia (JEMS'01).
[10] Berkov DV. Magnetization dynamics including thermal fluctuations: Basic phenomenology, fast remagnetization processes and transitions Over high-energy barriers. In: Handbook of magnetism and advanced magnetic materials. John Wiley & Sons, Ltd; 2007, http://dx.doi.org/10.1002/9780470022184.hmm204.
[11] Lepadatu S. Unified treatment of spin torques using a coupled magnetisation dynamics and three-dimensional spin current solver. Sci Rep 2017;7(1):1–12.
[12] Fredkin D, Koehler T. Hybrid method for computing demagnetizing fields. IEEE Trans Magn 1990;26(2):415–7. http://dx.doi.org/10.1109/20.106342.
[13] Hahn MB. Temperature in micromagnetism: Cell size and scaling effects of the stochastic Landau–Lifshitz equation. J Phys Commun 2019;3(7):075009. http://dx.doi.org/10.1088/2399-6528/ab31e6.
[14] Siracusano G, et al. Description of statistical switching in perpendicular STT-MRAM within an analytical and numerical micromagnetic framework. IEEE Trans Magn 2018;54(5):1–10. http://dx.doi.org/10.1109/TMAG.2018.2799856.